Published in final edited form as:
IEEE Trans Ultrason Ferroelectr Freq Control. 2012 January ; 59(1): 174–181. doi:10.1109/TUFFC.2012.2170.

Pulse Wave Imaging of the Human Carotid Artery: An *In Vivo* Feasibility Study

Jianwen Luo,
Ultrasound and Elasticity Imaging Laboratory, Department of Biomedical Engineering, Columbia University, New York, NY

Ronny X. Li, and
Ultrasound and Elasticity Imaging Laboratory, Department of Biomedical Engineering, Columbia University, New York, NY

Elisa E. Konofagou
Ultrasound and Elasticity Imaging Laboratory, Department of Biomedical Engineering, Columbia University, New York, NY. Department of Radiology, Columbia University, New York, NY

Elisa E. Konofagou: ek2191@columbia.edu

Abstract

Noninvasive quantification of regional arterial stiffness, such as measurement of the pulse wave velocity (PWV), has been shown to be of high clinical importance. Pulse wave imaging (PWI) has been previously developed by our group to visualize the propagation of the pulse wave along the aorta and to estimate the regional PWV. The objective of this paper is to determine the feasibility of PWI in the human carotid artery *in vivo*. The left common carotid arteries of eight (n = 8) healthy volunteers (male, age 27 ± 4 years old) were scanned in a long-axis view, with a 10-MHz linear-array transducer. The beam density of the scan was reduced to 16 beams within an imaging width of 38 mm. The frame rate of ultrasound imaging was therefore increased to 1127 Hz at an image depth of 25 mm. The RF ultrasound signals were then acquired at a sampling rate of 40 MHz and used to estimate the velocity of the arterial wall using a 1-D cross-correlation-based speckle tracking method. The sequence of the wall velocity images at different times depicts the propagation of the pulse wave in the carotid artery from the proximal to distal sides. The regional PWV was estimated from the spatiotemporal variation of the wall velocities and ranged from 4.0 to 5.2 m/s in eight (n = 8) normal subjects, in agreement with findings reported in the literature. PWI was thus proven feasible in the human carotid artery, and may be proven useful for detecting vascular disease through mapping the pulse wave and estimating the regional PWV in the carotid artery.

J. Luo is now with the Center for Biomedical Imaging Research and the Department of Biomedical Engineering, School of Medicine, Tsinghua University, Beijing, China (Jianwen@tsinghua.edu.cn.

I. Introduction

Aortic stiffness has been proven to be a strong independent predictor of all-cause and cardiovascular mortality, primary coronary events and fatal stroke in hypertensive patients [1]–[3], cardiovascular and all-cause mortality in end-stage renal disease [4] and in type 2 diabetes and glucose-tolerance-tested multiethnic population [5], recurrent acute coronary events in patients with ischemic heart disease [6], and coronary heart disease and stroke in a general population [7].

Various indices have been introduced to quantify arterial stiffness [8]–[11]. These include arterial distensibility, arterial compliance, Peterson's elastic modulus, Young's elastic modulus, stiffness index (β), and pulse wave velocity (PWV). Among these, PWV is "the most hallowed (and still probably the best)" measure of arterial stiffness [9]. The European Society of Hypertension and the European Society of Cardiology have recently recommended the use of the carotid-femoral pulse wave velocity as a favored measure of aortic stiffness for the management of arterial hypertension [12].

Pulse waves are flow velocity, pressure, and diameter waves generated at the ejection phase of the left ventricle [13]. In an idealized model, the propagation speed of the wave, i.e., the PWV, is directly related to the Young's modulus of the artery [13]. A higher PWV is associated with a stiffer artery. The PWV has been measured through a flow velocity wave, pressure wave, or diameter wave. In the conventional foot-to-foot method, i.e., the current gold standard, the waveforms at two measurement points in the arterial tree (typically, at the common carotid and femoral arteries) are obtained [8], [13]. The PWV is calculated as the distance between two measurement points divided by the time shift of the waveforms at the two points. Despite the simple definition of PWV, some problems in the methodology still remain, thus limiting the interpretation of available findings and the general applicability of the PWV measurement.

The accuracy of PWV measured from the foot-to-foot method suffers from errors of distance measurements and time-delay measurements [14], [15]. It is difficult to measure small time shifts, because the pulse wave travels very fast (on the order of several meters per second). A large time shift over a relatively long distance (e.g., between the common carotid and femoral arteries) is thus needed for reliable measurements. Therefore, the PWV measured represents a global and average value between two measurement sites. However, the stiffness of the arteries is nonuniform along the vasculature [13]. It is known that the stiffness of the arteries, and thus PWV, increase from the proximal to the distal regions [13]. In addition, the distance measurement is based on the assumption that the arterial wall does not change its geometry between the two measurement points, which may not always hold [8]. Large errors in the distance measurement may also increase when the two measurement points are far away because the arteries between these two points may not necessarily be uniform or straight, especially in aged subjects and patients with vascular diseases. Moreover, these points may not always lie along the path of travel of the pulse wave [16]. In the carotid and femoral arteries, for example, the pulse wave travels in opposite directions. Therefore, measurements of regional PWV, instead of global PWV, can be of great interest.

Several medical imaging-based methods have been previously developed for noninvasive measurements of regional PWV, mainly using magnetic resonance imaging (MRI) [17]–[21] and ultrasound [22]–[31]. Pulse wave imaging (PWI) was developed by our group as an ultrasound- based method for both qualitative visualization of the pulse wave propagation in real time [32] and quantitative estimation of regional PWV in both mice and human abdominal aortas [33]–[37]. One advantage of PWI over other PWV estimation methods is that the propagation patterns of the pulse wave can be visualized, in addition to obtaining a single PWV value. This information can be very useful for diagnosis of local vascular diseases such as abdominal aortic aneurysm (AA), as previously demonstrated by our group [35]. PWI has been validated with finite- element simulations [38], phantom experiments using mechanical testing [37], and healthy subjects using applanation tonometry [39]. Previous work on PWI has mainly been reported on the normal abdominal aorta and AA. In this paper, the feasibility of this method in the human carotid artery is demonstrated in healthy volunteers. Estimation of the regional stiffness of the carotid artery is of great clinical interest. For example, carotid artery atherosclerosis may lead to plaque rupture and eventually to stroke [40]. It is known that this geometrically focused disease is associated with regional changes in mechanical properties of the carotid artery such as stiffness, resulting in changes in the PWV [41].

II. Methods

A. Data Acquistion

As shown in Fig. 1(a), the longitudinal (long-axis) view of the left common carotid arteries of eight (n = 8) young healthy male subjects (age: 27 ± 4 years old) in the supine position was scanned using a SonixTOUCH system (Ultrasonix Medical Corp., Burnaby, BC, Canada) and a L14–5/38 linear array operating at 10 MHz. This study was approved by the Institutional Review Board (IRB) of Columbia University.

The image depth was fixed at 2.5 cm. Because the pulse wave travels at such a high speed (about 5 m/s), a high frame rate was necessary to visualize its propagation and estimate the PWV. By reducing the beam density in the ultrasound B-scan image from 128 to 16 beams with an image width of 38 mm, the frame rate of the ultrasonic images was increased from 140 to 1127 Hz, deemed to be sufficient for imaging of the pulse wave propagation [42]. The RF signals were digitized at a sampling frequency of 40 MHz. Before each data acquisition using 16 beams, B-mode images at a regular beam density (128 beams) were also acquired at a frame rate of 140 Hz for a duration of 0.2 s. The high-beam-density acquisition provided the reference B-mode image useful for segmentation of the anterior (near) wall of the carotid artery. The acquisition of high-beam-density images was immediately followed by 2.5 s of low-beam-density acquisition at nearly the same view, which generally included two cardiac cycles. A full acquisition (combining both high and low beam densities) lasted about 3 s, during which the subject was asked to hold his breath. About 5 acquisitions were performed to include approximately 10 cardiac cycles for each subject. The total time of acquisition was less than 20 s for each subject.

B. Data Processing

The incremental (interframe), axial displacements were estimated offline from the RF signals using 1-D normalized cross-correlation-based, real-time motion estimation method [32]. The window size was equal to 1.2 mm with a 75% overlap. The rigid motion induced by respiration and/or probe movements was removed by subtracting the displacements of the tissues located in the near field and at least 5 cm away from the arterial wall from the displacements of the carotid artery. The wall velocities were obtained by multiplying the estimated incremental displacements by the frame rate.

The estimated wall velocities were color-coded and overlaid onto the 2-D grayscale B-mode images acquired at a standard beam density (128 beams). Only the velocities on the anterior carotid wall and the peri-carotid tissue were shown for better visualization, i.e., after separation from lumen estimations. The anterior carotid wall was manually traced from the B-mode image at a regular beam density configuration. The sequence of wall velocity images was generated to form a ciné-loop.

The wall velocity variation with distance and time of the pulse-wave propagation was shown in a 2-D image, depicting the spatiotemporal variation of the pulse-wave propagation. The distance was calculated through manual tracing and was not necessarily equal to the image width because the carotid artery did not necessarily lie along the horizontal direction on the image.

On the 2-D spatiotemporal images, the foot (i.e., fiduciary point) of the wall velocity waveform was defined as the inflection point, at which the temporal derivative of the velocity (i.e., wall acceleration) attains its maximum before the peak velocity. The temporal derivative was calculated from the wall velocity waveform by using a 7-point low-pass Savitzky-Golay digital differentiator based on a piecewise least-square linear fitting [43]. The time of the foot (after beam-sweeping correction, described subsequently) was plotted against the distance traveled by the pulse wave. A linear regression fit was applied on the time-distance plot. The PWV was calculated as the reciprocal of the linear regression slope. The average PWV of each subject was then calculated from about 10 cardiac cycles.

The period of ultrasound beam sweeping was on the same order of magnitude as the time of pulse wave propagation. The beam sweeping period is equal to the inverse of the frame rate (i.e., 1127 Hz). In this study, it is equal to 0.89 ms. At an average PWV of 4.5 m/s, the time of pulse wave propagation across a 38-mm region is 8.4 ms. In this study, the direction of beam sweeping was always opposite to the direction of pulse-wave propagation. This configuration artificially increased the duration of pulse-wave propagation detected by PWI [Figs. 2(b) and 2(c)]. Beam sweeping induced artificial time delays between two successive lines that had to be corrected to ensure accurate PWV estimation. Such a correction was performed in the PWI acquisitions used here by subtracting the artificial time delays from the time delays detected by PWI.

III. Results

Fig. 2(a) is the B-mode image acquired with a high beam density (128 beams). Figs. 2(b)–2(d) show the wall velocity image of the carotid artery of a healthy volunteer (no. 5 in Table I) at different time instants, with a time interval of 3.5 ms (i.e., 4 frames). When the pulse wave arrives, the anterior wall undergoes upward motion while the posterior wall (i.e., far wall) undergoes downward motion (not shown). The arrows indicate the propagation of the pulse wave from the proximal (left, closer to the heart) to the distal (right, closer to the brain) sites along the carotid artery.

Fig. 3(a) illustrates the spatiotemporal variation of the wall velocity in the carotid artery. The horizontal axis represents time; the vertical axis represents the longitudinal positions of the carotid artery (i.e., distance from the proximal to distal regions) associated with different ultrasound beams. The circle indicates the fiduciary point, or foot, of the pulse wave at different longitudinal positions. The time delay between wall velocities at different positions is observed in Fig. 3(a). The amplitude of the downstream waveform is slightly larger than that for the upstream waveform [Fig. 3(a)]. This is mainly due to wave reflection in the upstream case [13].

The wall velocity waveforms in Fig. 3(c) are taken at three locations (A, B, and C) as indicated in Fig. 3(a). The inset in Fig. 3(c) shows the magnified waveforms near the time of pulse wave arrival. The time delay between wall velocity waveforms resulting from the propagation of the pulse wave is evident in Fig. 3(c).

Similar to Figs. 3(a) and 3(c), Figs. 3(b) and 3(d) show the spatiotemporal variation of the wall acceleration in the carotid artery and wall acceleration waveforms at the three locations, respectively. The propagation of the pulse wave can also be observed in Figs. 3(b) and 3(d).

From the spatiotemporal images of the pulse-wave propagation (Fig. 3), the time occurrence of the foot of the pulse wave is obtained at each beam position and shown in a scatter plot in Fig. 4. The vertical axis represents the relative time of the pulse wave, i.e., the time of peak velocity occurrence relative to the arrival time on the leftmost edge of the B-mode image. The horizontal axis represents the distance of the pulse wave, from the leftmost side of the B-mode image. The linear regression fit was applied to the plot of time (dependent variable) versus distance (independent variable). The PWV along the carotid artery is estimated as the inverse of the slope of the linear regression fit and is equal to 4.3 m/s in this case. The correlation coefficient (r) of the linear regression is 0.97, indicating high quality of the linear regression fit and uniform propagation of the pulse wave along the imaged segment of the carotid artery. For the same subject, approximately 10 cardiac cycles are used to calculate the average value and standard deviation (SD) of the PWV. In this case, the PWV is equal to 4.4 ± 0.3 m/s.

Table I shows the results obtained in all eight ($n = 8$) subjects. In the case of each subject, the average value and SD are calculated from approximately 10 cardiac cycles. The coefficient of variation (CV, defined as the ratio of the SD to the average PWV) ranges from 7 to 11%. The PWV in eight subjects ranged from 4.0 to 5.2 m/s. The correlation coefficient of the linear regression remains higher than 0.90 in all cases.

IV. Discussion

The carotid artery supplies oxygenated blood to the brain. Quantification of its stiffness information, such as measurement of the PWV, may be useful in the early diagnosis and characterization of vascular diseases such as carotid artery atherosclerosis. The conventional foot-to- foot method of the PWV measurement provides the average and global PWV between the carotid and femoral arteries. Estimation of the regional PWV may prove to be very helpful as a clinical biomarker.

PWI is a noninvasive, ultrasound-based method for visualization of the pulse wave propagation and quantitative estimation of regional PWV. In this paper, the feasibility of this technique in the carotid artery was shown in healthy subjects. From the sequence of wall velocity images (Fig. 2) and spatiotemporal variation of the wall velocities (Fig. 3), the propagation of the pulse wave along the carotid artery can be observed. The regional PWV estimation was obtained from a linear regression fit applied to the spatiotemporal variation of the pulse wave (Fig. 4). The measurements of the PWV in 8 healthy subjects (4.0 to 5.2 m/s) were in agreement with findings in the literature (4 to 6 m/s) [23], [31], [44], [45].

In the data acquisition, we first performed a 0.2-s high-beam- density acquisition, which provided the high-resolution reference B-mode image. The expansion of the artery causes a change of the region of the anterior (near) wall in position. In this study, the phase of the period of 0.2 s is arbitrary because we did not use ECG to trigger the data acquisition. However, the radial position of the anterior wall is not important in this study for several reasons. First, the movement of the arterial wall is relatively small. Second, the surrounding tissues moved together with the arterial wall. Therefore, the velocities in both the anterior carotid wall and the peri-carotid tissue were shown in Fig. 2. Third, the lateral position of the pulse wave (i.e., distance in Figs. 3 and 4) at a given time point is more critical in the PWV estimation. By assuming no or small lateral movement of the arterial wall, the lateral position was not affected by the expansion of the artery.

Only the velocity of the anterior wall was considered in this paper. When the pulse wave arrives, both the anterior and posterior walls of the carotid artery move outward radially, thus increasing the diameter of the artery. As a result, the anterior (near) wall undergoes an upward motion (Fig. 2) while the posterior (far) wall undergoes a downward motion (not shown). By subtracting the posterior-wall displacement (or velocity) from the anterior-wall motion, the distension (or distension velocity) waveform can be obtained, as other research groups have reported [23], [44]. In this study, however, the geometry of the carotid artery is not always horizontal throughout the image or along the lateral beam direction. In other words, the anterior and posterior walls along the same ultrasound beam locations are not necessarily within the same cross-section of the carotid artery. Therefore, their velocity waveforms may not be in phase during pulse wave propagation. To avoid any assumptions that must be made regarding the orientation of the carotid artery, as is done in other studies, only the anterior-wall velocity was considered in this study. However, the velocity of the anterior wall can still be affected by the rigid motion induced by respiration or probe movement. Therefore, in this study, the subjects were asked to hold their breath and the probe was held still. Any remaining rigid motion induced by respiration was further

minimized by subtracting the motion of the tissues located in the near field from the motion of the carotid artery. If significant rigid motion was still observed in the wall velocity images (Fig. 2) or spatiotemporal maps [Fig. 3(a)], those data were discarded in the estimation of PWV. Longitudinal movement of the carotid artery was not considered in this study. In the estimation of the time delay caused by pulse wave propagation, the phase of the wall velocity waveform was more important than its amplitude. For this reason, the longitudinal movement was expected not to significantly affect the estimation of time delay. However, the longitudinal translation will impact the distance measurement and thus the PWV estimate. This is, therefore, a limitation of this method.

The beam density was reduced to 16 beams to sufficiently increase the frame rate to accordingly map the propagation of the pulse wave. When a faster PWV is presented, such as in diseased carotid arteries, a higher frame rate is required to maintain the same accuracy of PWV estimation. At a given depth, the frame rate is inversely proportional to the beam density. The frame rate can be further increased if an even lower beam density (e.g., 8 beams) is used. At higher frame rates, the foot of the pulse wave can be easier to detect. In other words, the time delay between wall-velocity waveforms at different locations is larger in terms of frames and therefore can be estimated more accurately. However, the cost is the lower beam density and lateral resolution of the images. In addition, the PWV is estimated from the reciprocal of the slope of the linear regression fit. The reliability of the PWV estimation thus depends on the number of points in the linear regression fit. If fewer sample points are available, the linear regression fit does not have the required number of samples and becomes less reliable. A smaller number of data points (i.e., a lower beam density in this study) may increase the variation of the PWV estimation. In our preliminary comparison, the beam density of 16 beams provided a good tradeoff. However, the fundamental dependence of the upper limit of PWV on the frame rate and the optimum beam density for the lowest variation of the PWV estimation must be justified qualitatively and are currently being investigated in an ongoing parametric study with phantom experiments [46].

The foot of the wall velocity waveform was defined as the inflection point in the systolic phase, corresponding to the aortic valve opening. There are various definitions of the foot in the literature [26], [47], [48]. Hermeling *et al.* have recently shown that the dicrotic notch (also indicated in Fig. 3), which coincides with the aortic valve closure, provides a more robust measurement of the PWV than the systolic foot, as the latter can be influenced by the early wave reflection [44]. For the purpose of this feasibility study, only the systolic foot was considered. As shown in the spatiotemporal images of the wall velocities (Fig. 3), the forward and reflected waves are clearly separated, thus confirming the applicability of the use of systolic foot. However, a more thorough study on the quantitative comparison of different definitions of foot is warranted.

In addition to the PWV estimate, the propagation patterns of the pulse wave can be visualized with PWI. The high correlation coefficients of the linear regression fit (Table I) demonstrates the high quality of the regression fit and uniformity of the biomechanical proprieties of the common carotid arteries in healthy subjects. The uniform propagation of the pulse wave can also be observed in the sequence (Fig. 2) and the ciné-loop (not shown) of wall velocity images.

For the purpose of this feasibility study, only a limited number of healthy subjects were included in this study. In subsequent studies, we will test the capability of PWI in noninvasive characterization of local carotid disease such as carotid artery atherosclerosis and in the assessment of regional vascular damage caused by hypertension.

V. Conclusion

The feasibility of PWI in the human carotid artery was demonstrated in this paper. By reducing the beam density to 16 beams in a 38-mm-wide imaging window, the frame rate was increased to 1127 Hz, more than sufficient to image the propagation of the pulse wave and to estimate the regional PWV. The anterior wall velocity of the carotid artery was estimated from ultrasound RF signals. The regional PWV was then quantitatively estimated from the linear regression fit applied to the time–distance relationship of the pulse wave. The PWV in 8 healthy subjects was found to range from 4.0 to 5.2 m/s, which is in line with the values reported in the literature. The PWI method may thus provide important information on the distribution and quantification of the regional arterial stiffness of the human carotid artery, noninvasively and *in vivo*.

Acknowledgments

This work was supported in part by National Institutes of Health grants R01EB006042 and R01HL098830.

The authors wish to express their sincere thanks to J. Vappou, Ph.D., previously at Columbia University and currently at CNRS-Strasbourg University, France, for helpful discussions.

References

1. Laurent S, Boutouyrie P, Asmar R, Gautier I, Laloux B, Guize L, Ducimetiere P, Benetos A. Aortic stiffness is an independent predictor of all-cause and cardiovascular mortality in hypertensive patients. Hypertension. May; 2001 37(5):1236–1241. [PubMed: 11358934]
2. Boutouyrie P, Tropeano AI, Asmar R, Gautier I, Benetos A, Lacolley P, Laurent S. Aortic stiffness is an independent predictor of primary coronary events in hypertensive patients—A longitudinal study. Hypertension. Jan; 2002 39(1):10–15. [PubMed: 11799071]
3. Laurent S, Katsahian S, Fassot C, Tropeano AI, Gautier I, Laloux B, Boutouyrie P. Aortic stiffness is an independent predictor of fatal stroke in essential hypertension. Stroke. May; 2003 34(5):1203–1206. [PubMed: 12677025]
4. Blacher J, Safar ME, Guerin AP, Pannier B, Marchais SJ, London GM. Aortic pulse wave velocity index and mortality in end-stage renal disease. Kidney Int. May; 2003 63(5):1852–1860. [PubMed: 12675863]
5. Cruickshank K, Riste L, Anderson SG, Wright JS, Dunn G, Gosling RG. Aortic pulse-wave velocity and its relationship to mortality in diabetes and glucose intolerance—An integrated index of vascular function? Circulation. Oct; 2002 106(16):2085– 2090. [PubMed: 12379578]
6. Stefanadis C, Dernellis J, Tsiamis E, Stratos C, Diamantopoulos L, Michaelides A, Toutouzas P. Aortic stiffness as a risk factor for recurrent acute coronary events in patients with ischaemic heart disease. Eur Heart J. Mar; 2000 21(5):390–396. [PubMed: 10666353]
7. Sutton-Tyrrell K, Najjar SS, Boudreau RM, Venkitachalam L, Kupelian V, Simonsick EM, Havlik R, Lakatta EG, Spurgeon H, Kritchevsky S, Pahor M, Bauer D, Newman A, Hlth ABCS. Elevated aortic pulse wave velocity, a marker of arterial stiffness, predicts cardiovascular events in well-functioning older adults. Circulation. Jun; 2005 111(25):3384–3390. [PubMed: 15967850]
8. Laurent S, Cockcroft J, Van Bortel L, Boutouyrie P, Giannattasio C, Hayoz D, Pannier B, Vlachopoulos C, Wilkinson I, Struijker-Boudier H. Expert consensus document on arterial stiffness:

Methodological issues and clinical applications. Eur Heart J. Nov; 2006 27(21):2588–2605. [PubMed: 17000623]

9. O'Rourke MF, Staessen JA, Vlachopoulos C, Duprez D, Plante GE. Clinical applications of arterial stiffness; Definitions and reference values. Am J Hypertens. May; 2002 15(5):426–444. [PubMed: 12022246]
10. Van Bortel LM, Duprez D, Starmans-Kool MJ, Safar ME, Giannattasio C, Cockcroft J, Kaiser DR, Thuillez C. Clinical applications of arterial stiffness, Task force III: Recommendations for user procedures. Am J Hypertens. May; 2002 15(5):445–452. [PubMed: 12022247]
11. Pannier BM, Avolio AP, Hoeks A, Mancia G, Takazawa K. Methods and devices for measuring arterial compliance in humans. Am J Hypertens. Aug; 2002 15(8):743–753. [PubMed: 12160200]
12. Mancia G, De Backer G, Dominiczak A, Cifkova R, Fagard R, Germano G, Grassi G, Heagerty AM, Kjeldsen SE, Laurent S, Narkiewicz K, Ruilope L, Rynkiewicz A, Schmieder RE, Boudier H, Zanchetti A, Vahanian A, Camm J, De Caterina R, Dean V, Dickstein K, Filippatos G, Funck-Brentano C, Hellemans I, Kristensen SD, McGregor K, Sechtem U, Silber S, Tendera M, Widimsky P, Zamorano JL, Erdine S, Kiowski W, Agabiti-Rosei E, Ambrosioni E, Lindholm LH, Viigimaa M, Adamopoulos S, Agabiti-Rosei E, Ambrosioni E, Bertomeu V, Clement D, Erdine S, Farsang C, Gaita D, Lip G, Mallion JM, Manolis AJ, Nilsson PM, O'Brien E, Ponikowski P, Redon J, Ruschitzka F, Tamargo J, van Zwieten P, Waeber B, Williams B. 2007 guidelines for the management of arterial hypertension. J Hypertens. Jun; 2007 25(6):1105–1187. [PubMed: 17563527]
13. Nichols, WW.; O'Rourke, MF. McDonald's Blood Flow in Arteries. 5. New York, NY: Hodder Arnold; 2005.
14. Xu JP. Do we need a better approach for measuring pulse-wave velocity? Ultrasound Med Biol. Sep.2003 29(9):1373. [PubMed: 14553816]
15. Karamanoglu M. Errors in estimating propagation distances in pulse wave velocity. Hypertension. Jun.2003 41(6):E8. [PubMed: 12707295]
16. Hirata K, Kawakami M, O'Rourke MF. Pulse wave analysis and pulse wave velocity—A review of blood pressure interpretation 100 years after Korotkov. Circ J. Oct; 2006 70(10):1231–1239. [PubMed: 16998252]
17. Bolster BD, Atalar E, Hardy CJ, McVeigh ER. Accuracy of arterial pulse-wave velocity measurement using MR. J Magn Reson Imaging. Jul-Aug;1998 8(4):878–888. [PubMed: 9702890]
18. Boese JM, Bock M, Schoenberg SO, Schad LR. Estimation of aortic compliance using magnetic resonance pulse wave velocity measurement. Phys Med Biol. Jun; 2000 45(6):1703–1713. [PubMed: 10870719]
19. Macgowan CK, Henkelman RM, Wood ML. Pulse-wave velocity measured in one heartbeat using MR tagging. Magn Reson Med. Jul; 2002 48(1):115–121. [PubMed: 12111938]
20. Shao XZ, Fei DY, Kraft KA. Computer-assisted evaluation of aortic stiffness using data acquired via magnetic resonance. Comput Med Imaging Graph. Sep; 2004 28(6):353–361. [PubMed: 15294313]
21. Yu HY, Peng HH, Wang JL, Wen CY, Tseng WYI. Quantification of the pulse wave velocity of the descending aorta using axial velocity profiles from phase-contrast magnetic resonance imaging. Magn Reson Med. Oct; 2006 56(4):876–883. [PubMed: 16947380]
22. Brands PJ, Willigers JM, Ledoux LAF, Reneman RS, Hoeks APG. A noninvasive method to estimate pulse wave velocity in arteries locally by means of ultrasound. Ultrasound Med Biol. Nov; 1998 24(9):1325–1335. [PubMed: 10385955]
23. Meinders JM, Kornet L, Brands PJ, Hoeks APG. Assessment of local pulse wave velocity in arteries using 2D distension waveforms. Ultrason Imaging. Oct; 2001 23(4):199–215. [PubMed: 12051275]
24. Rabben SI, Stergiopulos N, Hellevik LR, Smiseth OA, Slordahl S, Urheim S, Angelsen B. An ultrasound-based method for determining pulse wave velocity in superficial arteries. J Biomech. Oct; 2004 37(10):1615–1622. [PubMed: 15336937]
25. Eriksson A, Greiff E, Loupas T, Persson M, Pesque P. Arterial pulse wave velocity with tissue Doppler imaging. Ultrasound Med Biol. May; 2002 28(5):571–580. [PubMed: 12079694]

26. Hermeling E, Reesink KD, Reneman RS, Hoeks APG. Measurement of local pulse wave velocity: Effects of signal processing on precision. Ultrasound Med Biol. May; 2007 33(5):774–781. [PubMed: 17383803]
27. Hoctor RT, Dentinger AM, Thomenius KE. Array signal processing for local arterial pulse wave velocity measurement using ultrasound. IEEE Trans Ultrason Ferroelectr Freq Control. May; 2007 54(5):1018–1027. [PubMed: 17523566]
28. Benthin M, Dahl P, Ruzicka R, Lindstrom K. Calculation of pulse-wave velocity using cross-correlation: Effects of reflexes in the arterial tree. Ultrasound Med Biol. 1991; 17(5):461–469. [PubMed: 1962347]
29. Hartley CJ, Taffet GE, Michael LH, Pham TT, Entman ML. Noninvasive determination of pulse-wave velocity in mice. Am J Physiol Heart Circ Physiol. Jul; 1997 273(1):H494–H500.
30. Williams R, Needles A, Cherin E, Zhou YQ, Henkelman RM, Adamson SL, Foster FS. Noninvasive ultrasonic measurement of regional and local pulse-wave velocity in mice. Ultrasound Med Biol. Sep; 2007 33(9):1368–1375. [PubMed: 17561330]
31. Couade M, Pernot M, Messas E, Emmerich J, Hagege A, Fink M, Tanter M. Ultrafast imaging of the arterial pulse wave. IRBM. Apr; 2011 32(2):106–108.
32. Luo J, Konofagou EE. A fast normalized cross-correlation calculation method for motion estimation. IEEE Trans Ultrason Ferroelectr Freq Control. Jun; 2010 57(6):1347–1357. [PubMed: 20529710]
33. Pernot M, Fujikura K, Fung-Kee-Fung SD, Konofagou EE. ECG-gated, mechanical and electromechanical wave imaging of cardiovascular tissues in vivo. Ultrasound Med Biol. 2007; 33(7):1075–1085. [PubMed: 17507146]
34. Fujikura K, Luo J, Gamarnik V, Pernot M, Fukumoto R, Tilson MD III, Konofagou EE. A novel, non-invasive technique for pulse-wave imaging and characterization of clinically significant vascular mechanical properties in vivo. Ultrason Imaging. 2007; 29(3):137–154. [PubMed: 18092671]
35. Luo J, Fujikura K, Tyrie LS, Tilson MD, Konofagou EE. Pulse wave imaging of normal and aneurysmal abdominal aortas in vivo. IEEE Trans Med Imaging. Apr; 2009 28(4):477–486. [PubMed: 19272985]
36. Wang S, Lee WN, Provost J, Luo J, Konofagou EE. A composite high-frame-rate system for clinical cardiovascular imaging. IEEE Trans Ultrason Ferroelectr Freq Control. Oct; 2008 55(10): 2221–2233. [PubMed: 18986870]
37. Vappou J, Luo J, Konofagou EE. Pulse wave imaging for noninvasive and quantitative measurement of arterial stiffness in vivo. Am J Hypertens. Apr; 2010 23(4):393–398. [PubMed: 20094036]
38. Vappou J, Zervantonakis IK, Luo J, Konofagou EE. Finite element modeling of the pulse wave propagation in the aorta for simulation of the pulse wave imaging (PWI) method. MICCAI Workshop Proc—Computational Biomechanics for Medicine III. 2008:118–127.
39. Vappou J, Luo J, Okajima K, Di Tullio M, Konofagou EE. Aortic pulse wave velocity measured by pulse wave imaging (PWI): A comparison with applanation tonometry. Artery Res. 2011; 5(2): 65–71. [PubMed: 24817917]
40. Lusis AJ. Atherosclerosis. Nature. Sep; 2000 407(6801):233– 241. [PubMed: 11001066]
41. van Popele NM, Grobbee DE, Bots ML, Asman R, Topouchian J, Reneman RS, Hoeks APG, van der Kuip DAM, Hofman A, Witteman JCM. Association between arterial stiffness and atherosclerosis—The Rotterdam study. Stroke. Feb; 2001 32(2):454–460. [PubMed: 11157182]
42. Sorensen GL, Jensen JB, Udesen J, Holfort IK, Jensen JA. Pulse wave velocity in the carotid artery. Proc IEEE Ultrason Symp. 2008:1386–1389.
43. Luo J, Ying K, He P, Bai J. Properties of Savitzky-Golay digital differentiators. Digit Signal Process. Mar; 2005 15(2):122– 136.
44. Hermeling E, Reesink KD, Kornmann LM, Reneman RS, Hoeks APG. The dicrotic notch as alternative time-reference point to measure local pulse wave velocity in the carotid artery by means of ultrasonography. J Hypertens. Oct; 2009 27(10):2028–2035. [PubMed: 19587605]
45. Kanai H, Umezawa A, Koiwat Y. Transcutaneous measurement of frequency dispersion in the regional pulse wave velocity. Proc IEEE Ultrasonics Symp. 2000:1281–1284.

46. Li RX, Luo J, Balaram SK, Chaudhry FA, Lantis JC, Shahmirzadi D, Konofagou EE. In-vivo pulse wave imaging for arterial stiffness measurement under normal and pathological conditions. Proc Int Conf IEEE Engineering Medicine and Biology Society. 2011:567–570.

47. Chiu YC, Arand PW, Shroff SG, Feldman T, Carroll JD. Determination of pulse-wave velocities with computerized algorithms. Am Heart J. May; 1991 121(5):1460–1470. [PubMed: 2017978]

48. Mitchell GF, Pfeffer MA, Finn PV, Pfeffer JM. Comparison of techniques for measuring pulse-wave velocity in the rat. J Appl Physiol. Jan; 1997 82(1):203–210. [PubMed: 9029217]

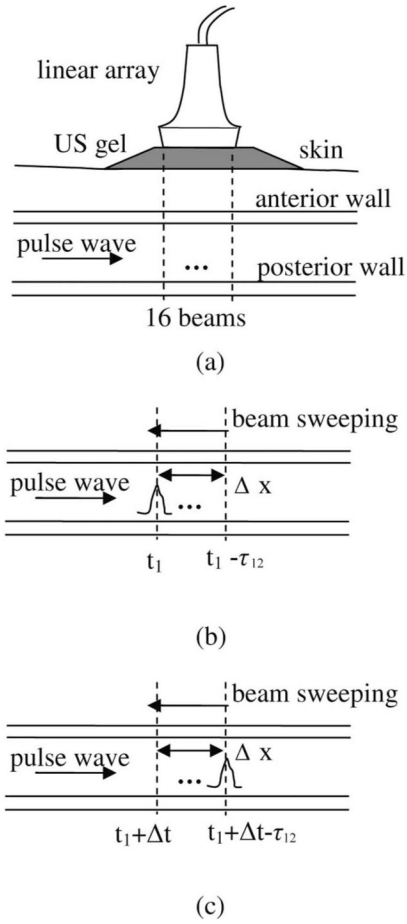

Fig. 1.

(a) Schematic diagram of the *in vivo* experiments. (b) and (c) show how beam sweeping affects the pulse wave velocity (PWV) estimation. (b) At time t_1, the pulse wave arrives at the leftmost beam. (c) Several (N) frames later, the pulse wave arrives at the rightmost beam. The distance between the leftmost and rightmost beams is Δx. The time delay between these two frames is Δt, equal to N/(frame rate). The true propagation time of the pulse wave is $\Delta t - \tau_{12}$, and the true PWV is $\Delta x/(\Delta t - \tau_{12})$, where τ_{12} is the time delay between the leftmost and rightmost beams resulting from beam sweeping. Without correction, the propagation time of the pulse wave is estimated as Δt (i.e., overestimated), and the PWV is estimated as $\Delta x/\Delta t$ (i.e., underestimated).

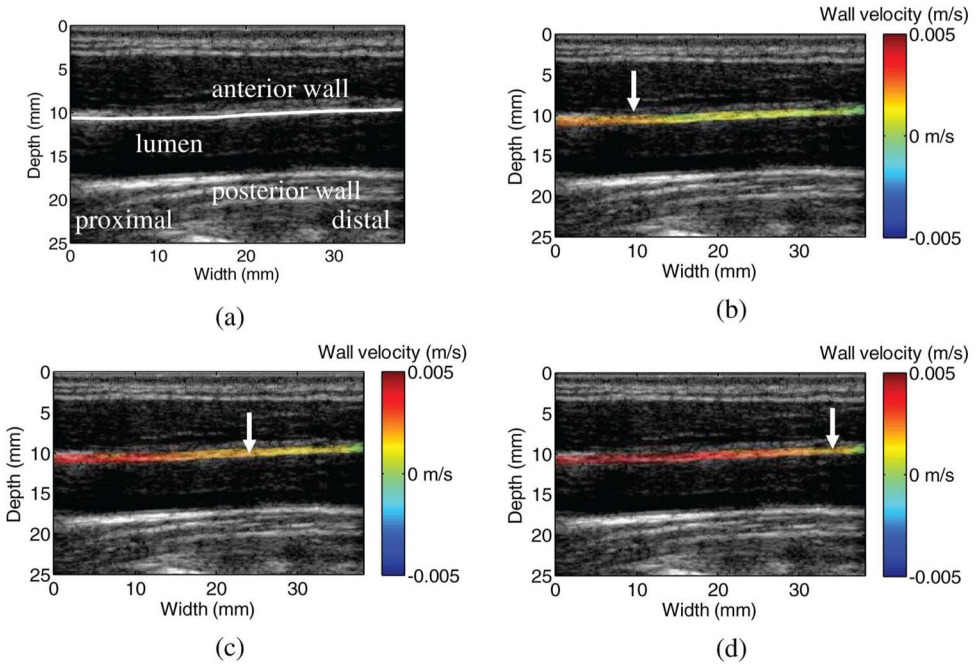

Fig. 2.

(a) A B-mode image and the (b)–(d) sequence of the wall velocity images in the left common carotid artery of a healthy volunteer. In (b)– (d), the wall velocities are color-coded and overlaid onto the B-mode image. Positive velocities (in red) represent upward motion, whereas negative velocities (in blue) represent downward motion. Only the velocities on the anterior wall of the carotid artery and the surrounding tissue are shown for better visualization. Images in (b)–(d) are 3.5 ms (i.e., 4 frames) apart. The solid arrows indicate the propagation of the pulse wave from the proximal (left) to the distal (right) sites (b)–(d). References to color refer to the online version.

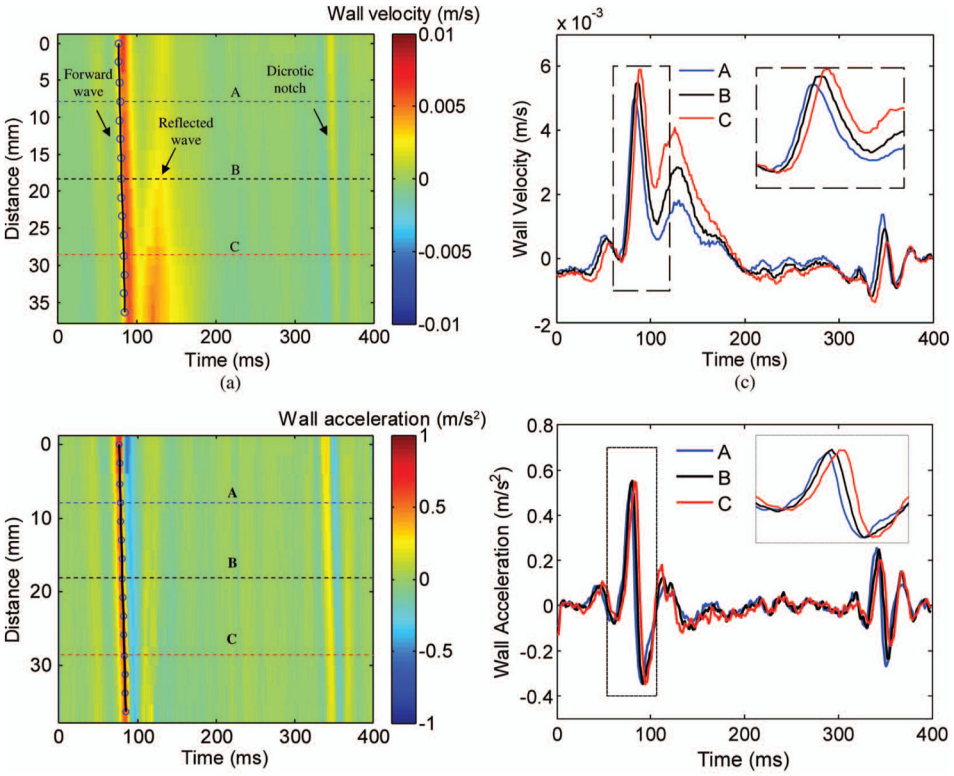

Fig. 3.

(a) Spatiotemporal variation of the wall velocity in the carotid artery, (c) wall velocity waveforms at three different locations, (b) spatiotemporal variation of the wall acceleration in the carotid artery, and (d) wall acceleration waveforms at three different locations. In (a) and (b), the horizontal axis represents time, whereas the vertical axis represents the longitudinal positions of the artery (from the proximal to the distal regions). The circles indicate the fiduciary point, or foot, of the pulse wave at different longitudinal positions. The linear fitting line near the circles indicates the delay of wall velocities or acceleration due to the pulse wave propagation. The wall velocity or acceleration waveforms in (c) and (d) were taken from the horizontal lines (A, B, and C) indicated in (a) and (b), respectively. The insets in (c) and (d) show the magnified waveforms of the regions indicated by the dashed rectangle.

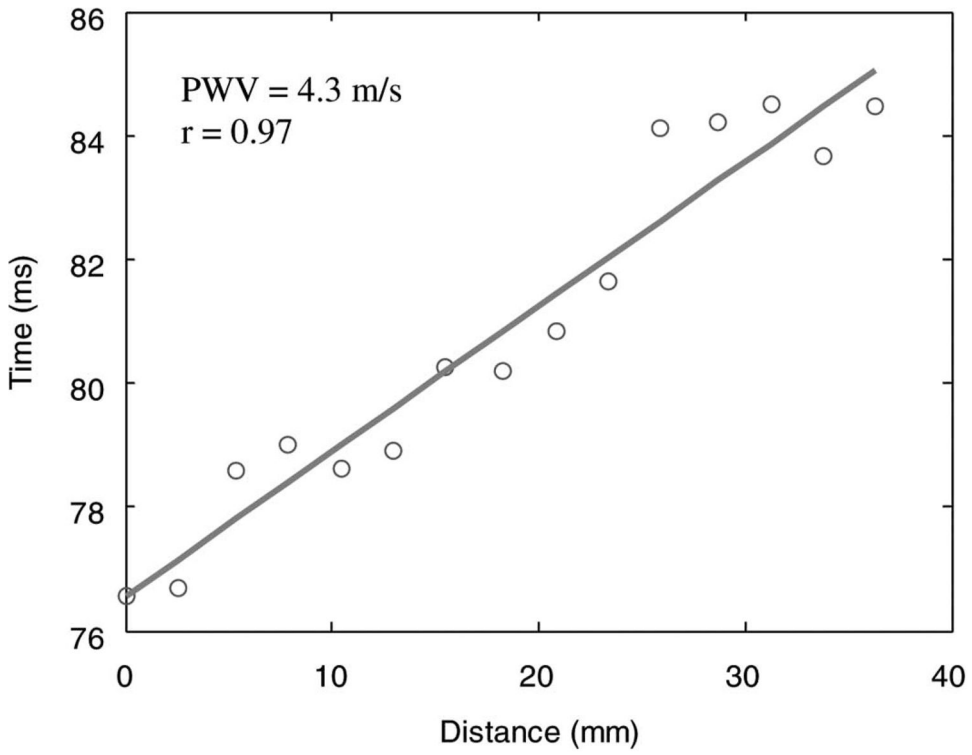

Fig. 4.

Time versus distance of the pulse wave propagation and the linear regression applied to them. The pulse wave velocity (PWV) is estimated as the reciprocal of the slope of the linear regression, and is equal to 4.3 m/s in this case. The correlation coefficient of the linear regress is 0.97.

TABLE I

Statistical Results of the Pulse Wave Imaging in 8 Healthy Volunteers.

Subject no.	Age	Pulse wave velocity (m/s)	Correlation coefficient (r)
1	22	4.5 ± 0.5	0.91 ± 0.05
2	28	4.3 ± 0.5	0.95 ± 0.03
3	23	4.1 ± 0.4	0.94 ± 0.04
4	24	5.2 ± 0.5	0.90 ± 0.06
5	32	4.4 ± 0.3	0.96 ± 0.02
6	32	4.4 ± 0.5	0.95 ± 0.02
7	25	4.8 ± 0.4	0.96 ± 0.03
8	26	4.0 ± 0.3	0.95 ± 0.02